


**Coordination Polymers** | *Hot Paper*

**Boronate Covalent and Hybrid Organic Frameworks Featuring P<sup>III</sup> and P=O Lewis Base Sites**

 Piotr Pacholak,<sup>[a]</sup> Krzysztof Gontarczyk,<sup>[a]</sup> Radosław Kamiński,<sup>[b]</sup> Krzysztof Durka,<sup>\*,[a]</sup> and Sergiusz Luliński<sup>\*,[a]</sup>

**Abstract:** Two covalent organic frameworks comprising Lewis basic P<sup>III</sup> centers and Lewis acidic boron atoms were prepared by poly-condensation reactions of newly obtained tris(4-diisopropoxyborylphenyl)phosphine with 2,3,6,7,10,11-hexahydroxytriphenylene and 2,3,6,7-tetrahydroxy-9,10-dimethylantracene. Obtained materials exhibit significant sorption of dihydrogen (100 cm<sup>3</sup> g<sup>-1</sup> at 1 bar at 77 K), methane (20 cm<sup>3</sup> g<sup>-1</sup> at 1 bar at 273 K) and carbon dioxide (50 cm<sup>3</sup> g<sup>-1</sup> at 1 bar at 273 K). They were exploited as solid-state ligands for coordination of Pd<sup>0</sup> centers. Alternatively, in

a *bottom-up* approach, boronated phosphine was treated with Pd<sub>2</sub>dba<sub>3</sub> and poly-condensated, yielding hybrid materials where the polymer networks are formed by means of covalent boronate linkages and coordination P–Pd bonds. In addition, the analogous materials based on phosphine oxide were synthesized. The DFT calculations on framework–guest interactions revealed that the behavior of adjacent boron and phosphorus/phosphine oxide centers is reminiscent of that found in Frustrated Lewis Pairs and may improve sorption of selected molecules.

**Introduction**


There is a continuous interest in covalent organic frameworks (COFs)—a class of porous organic materials composed of light elements such as carbon, boron, oxygen, nitrogen, silicon, and sulfur connected by strong covalent bonds.<sup>[1–6]</sup> Since the first report by Yaghi and co-workers in 2005,<sup>[7]</sup> numerous COF architectures were designed. From the structural topology point of view they can be divided in two major groups. Two-dimensional (2D) COFs are obtained from building blocks possessing planar structures.<sup>[8]</sup> In contrast, three-dimensional (3D) COFs are formed starting with precursors featuring a general 3D (e.g., tetrahedral) topology which imposes a structure of a resulting polymer network. Within this group, classical examples include highly porous materials such as COF-102 and COF-103


based on tetraboronic acids C[*p*-C<sub>6</sub>H<sub>4</sub>B(OH)<sub>2</sub>]<sub>4</sub> and Si[*p*-C<sub>6</sub>H<sub>4</sub>B(OH)<sub>2</sub>]<sub>4</sub>, respectively.<sup>[9]</sup>

The use of organophosphine linkers for the preparation of various multifunctional porous coordination polymers dates back to 2008. Since then, a number of materials were designed, especially by Humphrey and co-workers (phosphine coordination materials, PCMs).<sup>[10–25]</sup> It should be noted they generally comprise carboxylic groups coordinating metal secondary building units (SBUs). The pseudo-tetrahedral geometry around phosphorus centers favors the formation of 3D frameworks. The presence of lone electron pair at the P<sup>III</sup> centers provides a possibility for *pre*- or *post*-synthetic functionalization through alkylation,<sup>[16,26]</sup> arylation<sup>[27]</sup> or chalcogenation.<sup>[28]</sup> Such materials are also considered as solid-state ligands (SSLs) for coordination of transition metals.<sup>[12,29–35]</sup> Regarding the latter ability, the most common strategy involves the formation of robust coordination polymers with metals (Ca, Zr, Sc) weakly coordinated to phosphorus and hard-ligand donors (carboxylates, imidazolates, alkoxylates). In such porous networks, the softer phosphorus function allows the facile coordination of precious metal atoms including Pd<sup>0</sup>, Rh<sup>I</sup>, Ir<sup>I</sup>, Au<sup>I</sup>, Ag<sup>I</sup>, as well as low-valent Cu<sup>I</sup>, Co<sup>II</sup> metals. Importantly, their catalytic performance is usually retained from corresponding single-molecule phosphine-based catalysts. Thus, such materials offer a very attractive way to transfer catalytic processes from homogeneous to heterogeneous environments. This concept can also be used to achieve stronger and more selective binding of small-molecule substances, which can further be exploited for storage and separation processes. In addition to the P<sup>III</sup> materials, the analogous MOFs constituting phosphine oxide functions are obtained and used as a solid-state platforms for the lanthanide-metal coordination (La<sup>III</sup>, Dy<sup>III</sup>).<sup>[17,19]</sup>

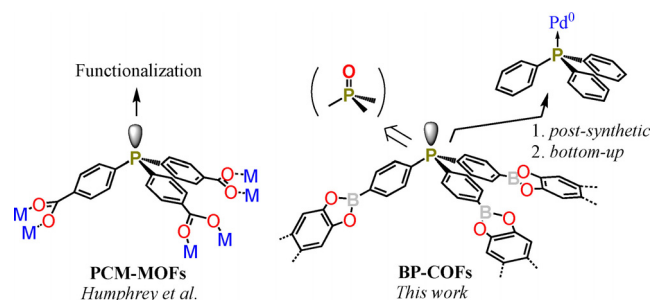
[a] P. Pacholak, Dr. K. Gontarczyk, Dr. K. Durka, Prof. S. Luliński  
Faculty of Chemistry  
Warsaw University of Technology  
Noakowskiego 3, 00-664 Warsaw (Poland)  
E-mail: kdurka@ch.pw.edu.pl  
serek@ch.pw.edu.pl

[b] Dr. R. Kamiński  
Department of Chemistry  
University of Warsaw  
Żwirki i Wigury 101, 02-089 Warsaw (Poland)

 Supporting information and the ORCID identification number(s) for the author(s) of this article can be found under:  
<https://doi.org/10.1002/chem.202001960>.

 © 2020 The Authors. Published by Wiley-VCH GmbH. This is an open access article under the terms of the Creative Commons Attribution License, which permits use, distribution and reproduction in any medium, provided the original work is properly cited.

Although the chemistry of PCM-MOFs is already well developed, the analogous COFs containing phosphine or phosphine oxide fragments have not been considered so far. Limited progress in this field was due to the lack of procedures allowing for the facile synthesis of phosphine-based COF precursors. In particular, boronated COFs are especially interesting due to the presence of weakly acidic boron centers along with stronger Lewis base phosphorus sites. In our efforts for the synthesis of functional porous materials<sup>[36,37]</sup> we have developed a new approach to synthesize boron-phosphine COFs (BP-COFs) (Scheme 1). Their non-planar tripodal topology is unique for all



**Scheme 1.** New class of COF materials based on boronated phosphines.

COF precursors. Thus, the prepared materials cannot be regarded as typical 3D COFs, which are based on nodes featuring the  $43m$  point-group symmetry. The presence of Lewis base  $P^{III}$  or  $P=O$  oxygen atoms and weakly acidic boron centers may significantly enhance the sorption properties of such materials. Furthermore, they can serve as a robust platform for the coordination of transition metals. Hence, in the current contribution we present *pre*- and *post*-synthetic modifications of COFs with palladium(0) using labile  $Pd_2dba_3$  complex as a metal source.

## Results and Discussion

Tris(4-bromophenyl)phosphine **1**, a starting material for the preparation of **2**, was obtained on a large scale (0.5 mol of the starting 1,4-dibromobenzene) from the metathesis of  $PCl_3$  with 4-bromophenyllithium according to the published procedure.<sup>[38]</sup> It was subjected to triple bromine–lithium exchange followed by a boronation with trialkyl borate reagent. After careful optimization, the approach based on the in situ addition of *t*BuLi (6 equiv) to the mixture of **1** and  $B(OiPr)_3$  in THF at  $-78^\circ C$  was found to give the best results (Figure 1 a). In our first attempts the reaction mixture was hydrolyzed in order to isolate tris(4-dihydroxyborylphenyl)phosphine **2a** as a precursor of COFs. However,  $^1H$  and  $^{31}P$  NMR analyses revealed that **2a** exists in equilibrium with its hydrated zwitterionic form (**2a'**) featuring protonated phosphorus atom and the anionic boronate group (Scheme S1, Supporting Information). Furthermore, we have observed its oxidation under air to corresponding phosphine oxide (**4a**), which is accompanied by a slow partial deboronation. Therefore, we decided to isolate com-

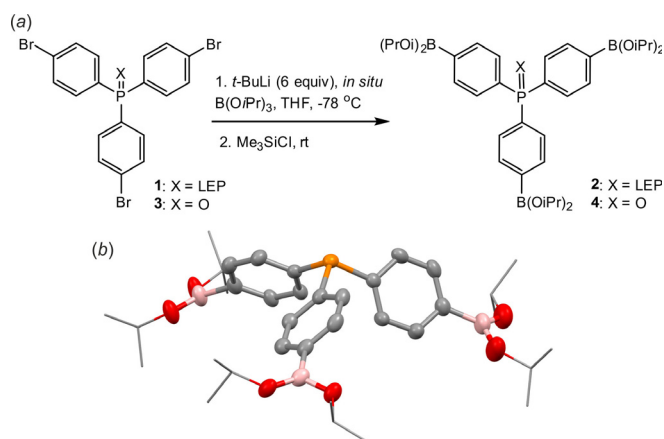


**Figure 1.** (a) Synthesis of triboronated phosphine **2** and phosphine oxide **4**. (b) The molecular structure of **2** (ellipsoids drawn at the 50% probability level, H-atoms and disordered sites omitted for clarity). LEP = Lone Electron Pair.

pound **2** by treating its tris(boronic) ate complex precursor with  $Me_3SiCl$  followed by removal of volatiles and extraction with heptane. Compound **2** was obtained in a pure form as colorless crystals in multigram quantities and reasonable yield (50%). The structure of **2** was confirmed by multinuclear NMR spectroscopy and X-ray diffraction (Figure 1 b). Notably, the crystal structure lacks intermolecular interactions between Lewis acidic boron atoms and Lewis base phosphorus centers.

The synthesis of boronated triphenylphosphine oxide precursor **4** involved the in situ Br/Li exchange/boronation of brominated precursor **3**<sup>[39]</sup> using the protocol analogous to that described for **2**. Compound **3** was isolated as a yellow solid and characterized by  $^1H$ ,  $^{11}B$  and  $^{31}P$  NMR spectroscopy. Unlike **2**, it is only sparingly soluble in  $CDCl_3$ , presumably due to extensive aggregation in solid state through the  $P=O \rightarrow B$  dative bonds.

As shown in Figure 2a the syntheses of materials **BP1–2** were performed by polycondensation reactions of **2** with 2,3,6,7,10,11-hexahydroxytriphenylene (HHTP, 1 equiv), or 2,3,6,7-tetrahydroxy-9,10-dimethylantracene (THDMA, 1.5 equiv), respectively. A general protocol similar to those developed for the preparation of other boronate ester COFs was employed.<sup>[1,2,6–9]</sup> Thus, a stoichiometric mixture of **2** and a polyol was stirred in a 1:1 (v/v) mesitylene – 1,4-dioxane mixture at  $85^\circ C$  followed by repeated washing of a crude product with anhydrous THF and final drying under high vacuum at  $150^\circ C$ . The prepared materials are grayish-green (**BP1**) or olive-green (**BP2**) powders. Their hydrolytic degradation in wet  $[D_6]DMSO$  (with added  $D_2O$ ) and  $^1H$  NMR analyses of resulting samples showed that their composition was in agreement with the theoretical stoichiometry. Since the precursor **2** is not the boronic acid but the respective ester, its poly-condensation reactions with HHTP and THDMA can be classified as transesterification-based processes. We suggest they should proceed more easily and faster than dehydrative poly-condensation reactions which occur during formation of COFs from free boronic acids and are typically conducted solvothermally although some examples involving mild conditions were reported.<sup>[40]</sup>

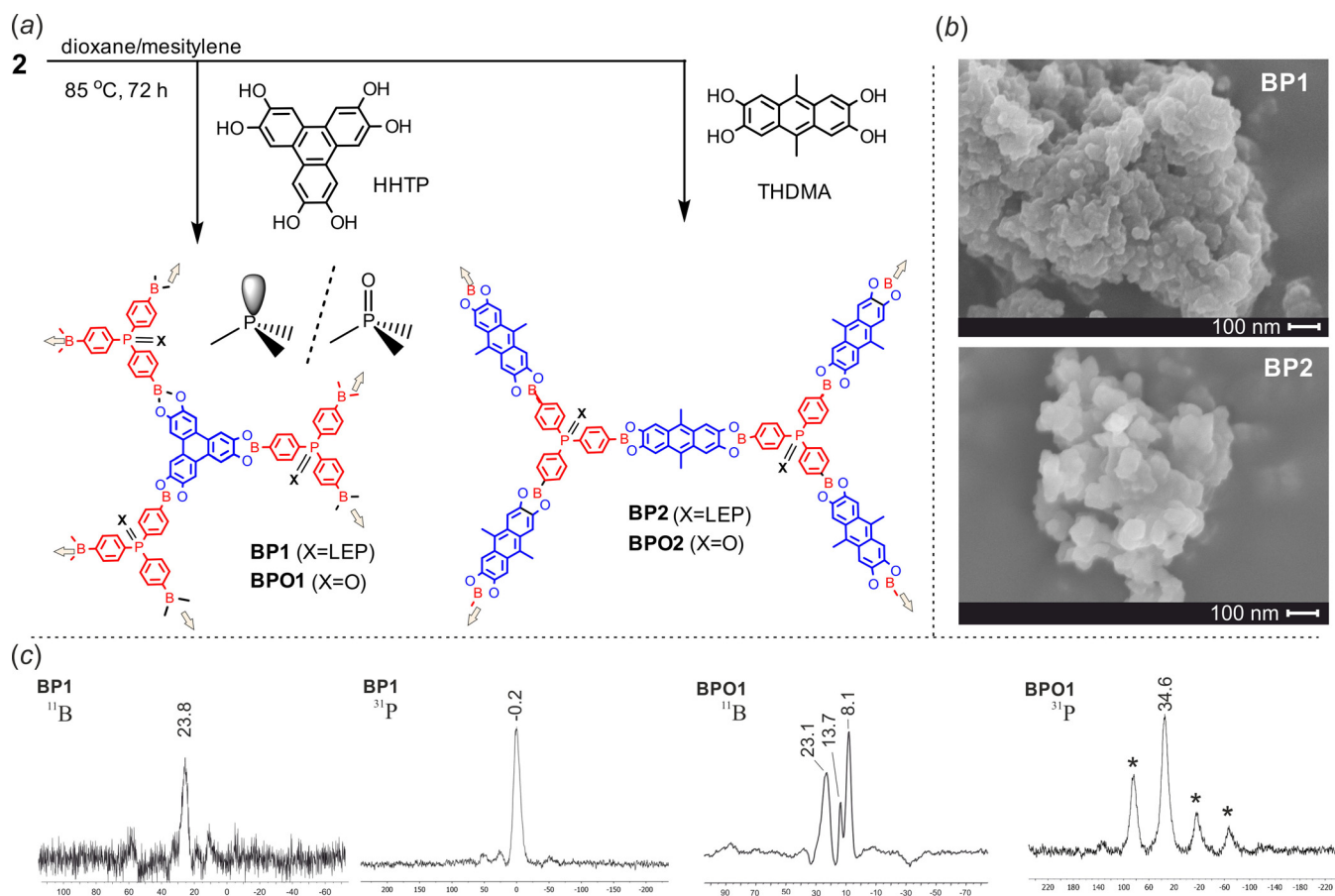


**Figure 2.** (a) Synthesis of **BP1-2** and **BPO1-2** porous materials. (b) SEM images of **BP1-2**. (c)  $^{11}\text{B}$  and  $^{31}\text{P}$  MAS NMR spectra of **BP1** and **BPO1** recorded at the spinning rate of 10 kHz. Asterisks (\*) indicate peaks arising from spinning side bands.

Thus, the synthesis of **BP1-2** was repeated at room temperature and both materials were obtained in good yields. Furthermore, their composition and appearance is very similar to the samples obtained with the heating applied. On the other hand, high reaction rates favor amorphization. Following the same protocol the synthesis of phosphine oxide-based materials (**BPO1-2**) was performed by poly-condensation reactions of **4** with HHTP (1 equiv) or THDMA (1.5 equiv), respectively.

In the next step, hybrid materials containing  $\text{Pd}^0$  metal centers were prepared utilizing two general strategies: (a) *bottom-up* approach involving  $\text{Pd}^0$  coordination to the precursor **1**, followed by polycondensation with HHTP/THDMA (**BP1-Pd(BU)**, **BP2-Pd(BU)**), (b) *post-synthetic* modification of previously obtained **BP1-2** COFs (**BP1-Pd(PS)**, **BP2-Pd(PS)**). It should be noted that the modification of organoboron polymers through metal complexation is still rather unexplored.<sup>[41]</sup> The synthesis of **BP1-Pd(BU)** and **BP2-Pd(BU)** was performed in two steps as shown on Figure 3a. At first, compound **2** was treated with  $\text{Pd}_2(\text{dba})_3$  at low temperature (ca.  $-50^\circ\text{C}$ ) in DCM. The amounts of starting materials were taken to achieve the Pd:P ratio of 1:4.

Initially, the reaction mixture had a purple color due to the presence of dissolved  $\text{Pd}_2(\text{dba})_3$ . However, a solution gradually turned olive-brown on warming to ambient temperature indicating the progress of ligand exchange at the Pd atom and for-

mation of a species of assumed stoichiometry  $\text{Pd}[\mathbf{2}]_4$  although it may equilibrate with  $\text{Pd}[\mathbf{2}]_2$  and/or  $\text{Pd}[\mathbf{2}]_3$  as well as free ligand **2**. The  $^{31}\text{P}$  NMR spectrum of this species showed a few resonances in the range of 24–26 ppm which confirms the formation of Pd-P dative bonds.<sup>[42]</sup> In the second step, the ob-

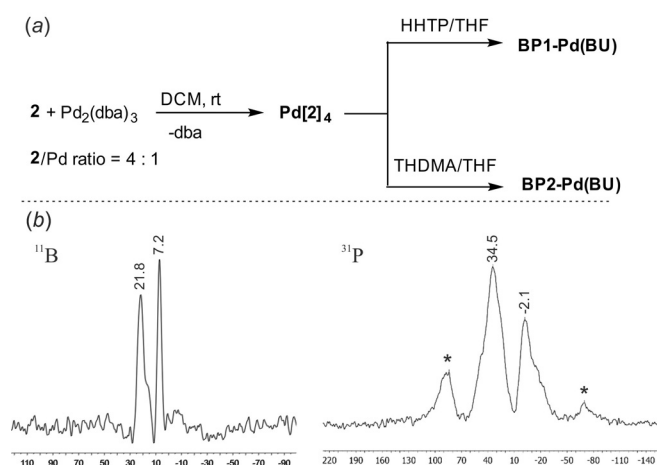


**Figure 3.** (a) Synthesis of Pd-functionalized COF materials using bottom-up approach. (b)  $^{11}\text{B}$  and  $^{31}\text{P}$  MAS NMR spectra of **BP1-Pd(BU)** recorded at the spinning rate of 10 kHz. Asterisks (\*) indicate peaks arising from spinning side bands.

tained complex was treated with a THF solution of a polyhydroxy linker, i.e., HHTP or THDMA, in a stoichiometric proportion with respect to **2**. The gradual precipitation of a voluminous brownish or olive-green precipitate was observed during several hours. The slurry was stirred for 3 days at room temperature and filtered under argon followed by thorough washing of a solid with several portions of anhydrous DCM. Drying under high vacuum at 80 °C resulted in final materials as free-flowing dark-colored powders. Analysis of a yellow filtrate revealed the presence of free ligand (dba) in amounts slightly less (ca. 15%) than those initially added with the used Pd precursor. It was not significantly contaminated by other compounds including boronated triphenylphosphine derivatives and polyhydroxy linkers, which indicates their quantitative incorporation in the bulk materials.

In the second approach, **BP1–2** materials were immersed in Pd<sub>2</sub>dba<sub>3</sub>/THF solution during 3 days. We assumed that the labile character of the complex should result in the attachment of Pd<sup>0</sup> to P centers<sup>[43,44]</sup> on the surface of pores having size sufficient for penetration with Pd<sub>2</sub>dba<sub>3</sub>. In both cases, the purple solution containing the unreacted complex was removed and the resulting materials were washed thoroughly with DCM and dried under vacuum (10<sup>−3</sup> torr, 50 °C) to give the final products **BP1-Pd(PS)** and **BP1-Pd(PS)** as dark powders.

The thermal stability of **BP1–2** (dried at 150 °C prior to analysis) was investigated under N<sub>2</sub> atmosphere by TGA technique (Figure S1). A minor mass loss (up to 5%) is observed up to 350 °C. It can be associated with the removal of adsorbed gases, and some volatile impurities (e.g., traces of solvents or by-products resulting from completion of condensation reactions). A gradual decomposition starts as the total mass loss at 600 °C reaches ca. 40% for both COF materials. To summarize, obtained boronate ester COFs exhibits comparably high thermal resistance consistent with the exclusive presence of strong covalent bonds. The presence of Pd nodes did not affect the thermal stability of **BP2-Pd(BU)** as the decomposition started also at ca. 350–400 °C (Figure S2). In turn, **BP1-Pd(BU)** material losses about 15% of its mass when heating up to 200 °C, which is probably associated with the presence of significant amount of solvent and dba molecules resided in the porous framework.

<sup>11</sup>B MAS NMR spectrum of **BP1** (Figure 2c) shows the resonance at ca. 24 ppm, i.e., in the range characteristic for trigonal boron atoms in arylboronic acids and esters.<sup>[45]</sup> The <sup>31</sup>P MAS NMR spectrum of **BP1** shows a sharp resonance at ca. 0 ppm, i.e., shifted downfield by ca. 6 ppm with respect to PPh<sub>3</sub>.<sup>[46]</sup> Very similar <sup>11</sup>B and <sup>31</sup>P MAS NMR spectra were recorded for **BP2** (see Supporting Information, Figures S23, S24). Based on these results one can conclude that the plausible structure stabilization of **BP1–2** due to formation of strong dative interactions between boron and phosphorus atoms should be excluded. However, a slight deshielding (relative to PPh<sub>3</sub>) of <sup>31</sup>P MAS NMR signals for both materials might indicate occurrence of weak communication between boron and phosphorus centers.<sup>[47]</sup> The <sup>11</sup>B MAS NMR spectrum of **BPO1** (Figure 2c) shows the resonances at 8.1, 13.7, 23.1 ppm. The latter can be assigned to the trigonal boron atom featuring CBO<sub>2</sub> environment

whereas two remaining ones may indicate that some boron atoms are coordinated with oxygen atoms of P=O groups and/or THF guest molecules. The <sup>31</sup>P MAS NMR spectrum of **BPO1** is characterized by persistence of intense spinning sidebands indicating that the chemical shift anisotropy frequency range is larger than the MAS rate. The spectrum has one isotropic chemical shift at 34.6 ppm consistent with the presence of triphenylphosphine oxide motifs. Very similar <sup>11</sup>B and <sup>31</sup>P MAS NMR spectra were recorded for **BPO2** (Figures S25, S26), thus confirming that the change of the linker topology does not significantly influence the <sup>31</sup>P NMR chemical shift anisotropy characteristics of the studied nuclei. <sup>11</sup>B MAS NMR spectra of the hybrid **BP1-Pd(BU)** and **BP2-Pd(BU)** materials (Figure 3b) are in general analogous to those recorded for **BPO1–2** as they point to dative interactions between some boron atoms and oxygen-based donors including remaining THF or dba molecules. The <sup>31</sup>P MAS NMR spectrum of **BP1-Pd(BU)** features a set of spinning sidebands with isotropic chemical shifts at −2.1 and 34.5 ppm (similar values of −0.7 and 36.3 ppm were recorded for **BP2-Pd(BU)**). The former one can be assigned to free triphenylphosphine moieties which indicates that P<sup>III</sup> nodes characteristic for **BP1** are also present in **BP1-Pd(BU)** to a significant extent. However, the latter more intense (ca. two-fold) signal can be assigned to triarylphosphine P atoms engaged in Pd–P dative bonds.<sup>[48]</sup> It should be noted that the presence of P–Pd coordination is also supported by XPS data which are discussed below.

Scanning electron microscopy (SEM) indicates mesoporous morphology of **BP1–2** (Figure 2b). This material forms sponge-like agglomerates of irregular shape and dimensions in the range of 0.5–20 μm. The size of particles (presumably nanocrystallites) forming these structures are very small and ranges from 50–200 nm. The impregnation of such a COF structure with palladium centers does not change the general morphology of the structure (Figure S41).

XPS analysis was employed to evaluate the amount of Pd centers adsorbed on the surfaces of COF materials obtained using *bottom-up* and *post-synthetic* methodologies. The survey of XPS spectra is shown in Figures S29–S32 in Supporting Information. Pd 3d and P 2p high-resolution XPS spectra of **BP1-Pd(BU)** and **BP1-Pd(PS)** COFs are shown in Figure 4, while the C1s, B1s, and O1s HR-XPS spectra regions and analogous spectra for **BP2**-derived hybrid materials are placed in the SI (Figures S33–S36).<sup>[49]</sup> As indicated by the analysis of Pd 3d region, two different Pd species can be distinguished. The doublet at binding energies (B.E) of 341.5 eV (Pd 3d<sub>3/2</sub>) and 336.3 eV (Pd 3d<sub>5/2</sub>) can be assigned to bulk palladium nanoparticles—(**Pd**(bulk), Table 1).<sup>[50]</sup> The bigger doublet is shifted towards higher binding energies (B.E=343.2 eV, 337.9 eV) and is associated with palladium centers coordinated to phosphorus atoms (Ar<sub>3</sub>P-Pd).<sup>[51]</sup> The appearance of metallic palladium on the COF surface results from the relatively low stability of Pd<sub>2</sub>(dba)<sub>3</sub> precursor and may indicate that its decomposition followed by formation of Pd clusters is catalyzed by the COF surface. The deconvolution of XPS curves clearly shows that total amount of Pd atoms adsorbed in the **BP1-Pd(BU)** and **BP2-Pd(BU)** materials is much lower with respect to *post-syn-*

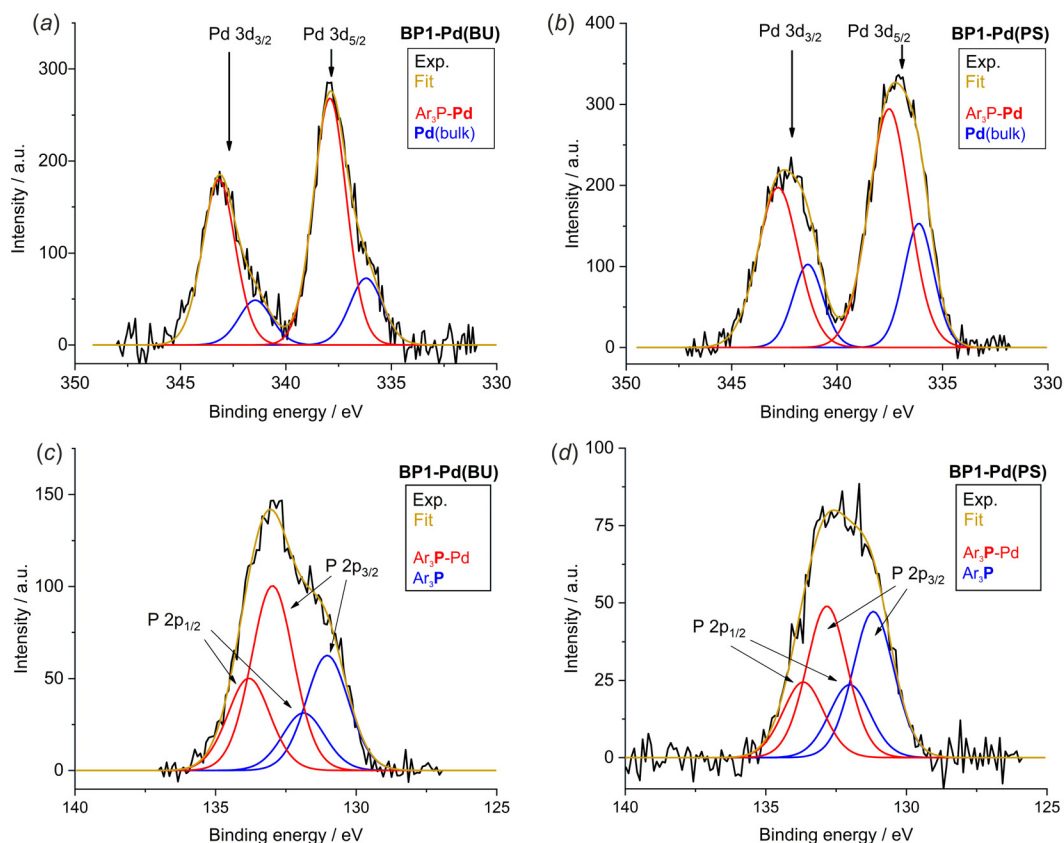


**Figure 4.** High-resolution XPS spectra for **BP1-Pd(BU)** (a, c) and **BP1-Pd(PS)** (b, d): Pd 3d (a, b) and P 2p (c, d).

**Table 1.** XPS-derived phosphorus and palladium atom amounts located on the surface of corresponding COF materials. **Pd(bulk)** and **Pd-P** denote bulk and bonded palladium atoms, **Ar<sub>3</sub>P** and **Ar<sub>3</sub>P-Pd** correspond to three-coordinate and Pd-bonded P atoms, respectively. Values are provided in atomic percent. The respective molar ratios are given below.

	<b>BP1-Pd(BU)</b>	<b>BP2-Pd(BU)</b>	<b>BP1-Pd(PS)</b>	<b>BP2-Pd(PS)</b>
<b>Pd(bulk)</b>	0.05	0.08	0.23	0.75
<b>Pd-P</b>	0.32	0.25	0.62	0.63
<b>Ar<sub>3</sub>P</b>	0.64	0.66	0.72	0.83
<b>Ar<sub>3</sub>P-Pd</b>	1.03	0.98	0.75	0.71
<b>Pd-P/Pd(bulk)</b>	6.40	3.13	2.70	0.84
<b>Ar<sub>3</sub>P-Pd/Ar<sub>3</sub>P</b>	1.61	1.48	1.04	0.85
<b>Ar<sub>3</sub>P-Pd/Pd-P</b>	3.22	3.9	1.21	1.13

thetically impregnated COFs, which is consistent with stoichiometry of P/Pd centers in precursors. Furthermore, the Pd-P/Pd(bulk) molar ratio is much lower for latter systems, specifically in case of **BP2-Pd(PS)** Pd bulk atoms outnumber those bound to P atoms. The deconvolution of P 2p core level spectra for **BP1-Pd(BU)** gives two doublets representing two set of P 2p<sub>1/2</sub> and P 2p<sub>3/2</sub> peaks. The peaks at 131.0 eV and 131.9 eV correspond to P atoms bound to three aromatic rings of the COF framework (**Ar<sub>3</sub>P**). The adjacent peaks at higher binding energies (B.E = 133.0 eV and 133.8 eV) can be attributed to the P centers coordinating palladium atoms (**Ar<sub>3</sub>P-Pd**). The comparison of Pd-containing materials obtained using either *bottom-*

*up* or *post*-synthetic approaches shows that proportion of free and bound P atoms is different in both material classes. In the former materials, the molar ratio of palladated vs. free phosphine (**Ar<sub>3</sub>P-Pd/Ar<sub>3</sub>P**) is close to 1.5 indicating that more than half of P atoms is bound to Pd, while in the case of *post*-synthetically modified COFs, this ratio is close to 1. Finally, as suggested by the molar ratio of coordinated P and Pd sites (**Ar<sub>3</sub>P-Pd/Pd-P**), in the case of **BP1-Pd(BU)** and **BP2-Pd(BU)** each Pd center is bound to 3 or 4 P atoms. Thus, these COFs preserve the stoichiometry of its precursor **Pd[2]<sub>4</sub>** and can be treated as mixed-hybrid networks composed of covalently linked organo-boron network interconnected by tetra-coordinated palladium centers. In turn, for **BP1-Pd(PS)** and **BP2-Pd(PS)** the molar ratio **Ar<sub>3</sub>P-Pd/Ar<sub>3</sub>P** is close to 1, which indicates that the structure of these materials is mostly preserved from initial **BP1–2** COFs. Overall, it can be concluded that the *post*-synthetically Pd-functionalized COFs are more preferred for catalytic applications, where the density of the catalytic centers plays the major role, while the palladium centers would be more dispersed and electronically active in materials obtained from a bottom-up approach.

The porosity of all obtained materials was initially evaluated using N<sub>2</sub> gas adsorption at 77 K. Prior to the measurements, samples were activated by heating at 150 °C under high vacuum (10<sup>-3</sup> torr) for 24 hours to remove any possible guest molecules. All recorded isotherms show a sharp increase of N<sub>2</sub> uptake at low relative pressures (below 0.02 P/P<sub>0</sub>) which is

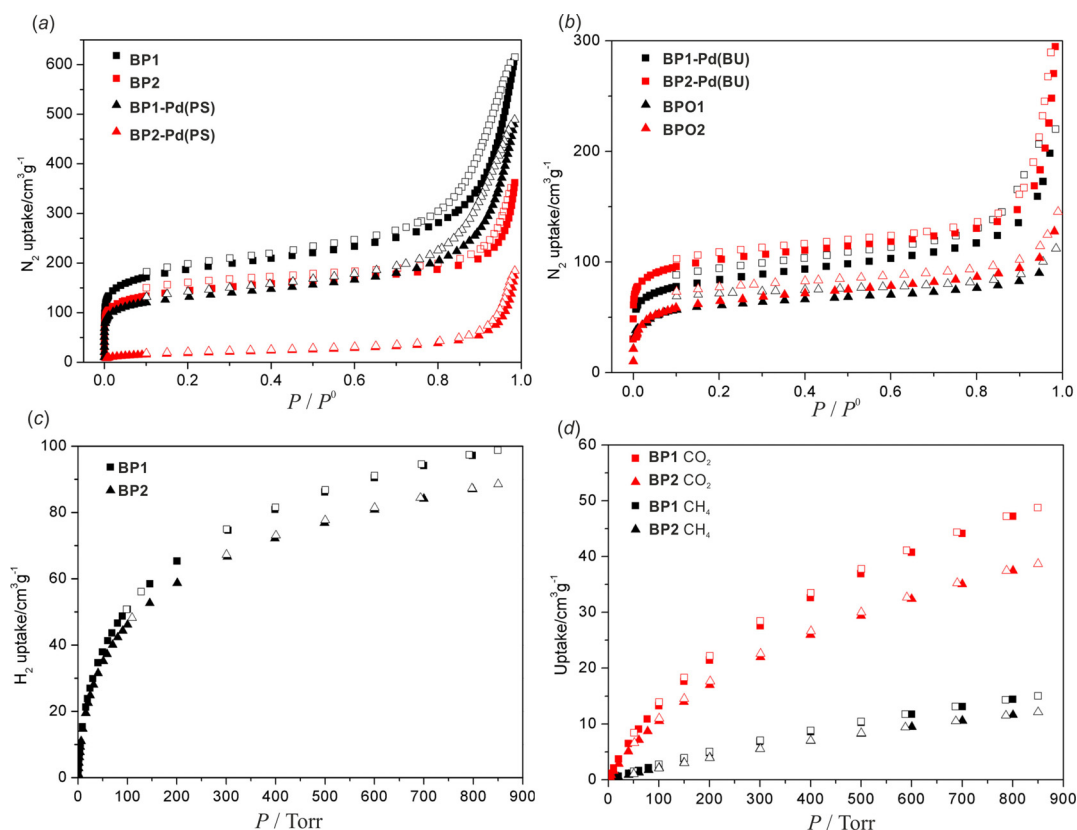


**Figure 5.** (a, b)  $N_2$  sorption isotherms (@77 K) for studied porous materials. (c)  $H_2$  (@77 K), (d)  $CO_2$  and  $CH_4$  (@273 K) sorption isotherms for **BP1–2**.

common for microporous materials (Figure 5a,b) including classical boron COFs. All studied materials exhibit similar type-II sorption isotherms with relatively slow and almost constant increase of sorption in the 0.05–0.8  $P/P_0$  pressure range. **BP1** shows the highest  $N_2$  uptake reaching ca.  $650 \text{ cm}^3 \text{ g}^{-1}$  STP. The  $N_2$  sorption is significantly decreased (to ca.  $200 \text{ cm}^3 \text{ g}^{-1}$  STP at  $P=P_0$ ) for the **BP1-Pd(BU)** hybrid material. On the other hand, both materials based on THDMA have similar  $N_2$  sorption properties (up to ca.  $300 \text{ cm}^3 \text{ g}^{-1}$  at  $P=P_0$ ) which suggests that the porosity is not significantly affected by introduction of Pd coordination centers. In addition, desorption measurements revealed that the isotherms are almost reversible for these two materials. For **BP1** and **BP1-Pd(BU)**, a more distinctive hysteresis loop was observed which may indicate the occurrence of capillary condensation within mesopores, due to the strength of adsorbate-adsorbent and adsorbate-adsorbate interactions.<sup>[52]</sup>

The Brunauer–Emmett–Teller model was used to calculate the relevant parameters including apparent surface area  $S_{\text{BET}}$  based on the Rouquerol’s consistency criteria,<sup>[53]</sup> and the pore volume  $V_p$  at  $P/P_0=0.98$  (Table 2). The  $S_{\text{BET}}$  value for **BP1** was significantly higher ( $669 \text{ m}^2 \text{ g}^{-1}$ ) than the remaining materials ( $72\text{--}532 \text{ m}^2 \text{ g}^{-1}$ ). Obtained results are comparable with those reported for related boron 2D COFs such as COF-1, COF-5,<sup>[6]</sup> and BTP-COF.<sup>[54]</sup>

We have also studied  $H_2$ ,  $CO_2$  and  $CH_4$  sorption for **BP1–2** (Figure 5c,d) as we hypothesized that the presence of Lewis acidic (B atoms) and Lewis basic (P atom) centers may be beneficial for selectivity of obtained materials due to synergistic effects. Specifically, highly inhomogeneous electric field could enhance interactions with molecules featuring polar bonds such as  $CO_2$ , but may also induce bond polarization in homoeatomic molecules such  $H_2$ . Both materials exhibit type-I sorption of  $H_2$ @77 K which is not saturated at  $P=P_0$ . The  $H_2$  uptake for

**Table 2.** Summary of surface areas,  $S_{\text{BET}}$ , gas uptakes and total pore volumes,  $V_p$  for all studied COF materials.

	<b>BP1</b> <sup>[a]</sup>	<b>BP2</b> <sup>[a]</sup>	<b>BPO1</b>	<b>BPO2</b>	<b>BP1-Pd(PS)</b>	<b>BP2-Pd(PS)</b>	<b>BP1-Pd(BU)</b>	<b>BP2-Pd(BU)</b>
$S_{\text{BET}}$ [ $\text{m}^2 \text{ g}^{-1}$ ]	669(703)	532(480)	235	245	485	71	310	383
$V_p$ [ $\text{cm}^3 \text{ g}^{-1}$ ]	0.95(0.48)	0.56(0.55)	0.17	0.22	0.76	0.30	0.34	0.49
$N_2$ @77 K, $P/P_0=0.98$	615.1(310.6)	362.0(358.1)	112.2	145.4	489.2	184.2	220.0	316.5
$H_2$ @77 K, $P=850$ torr	98.7(111.5)	88.5(68.6)	64.3	77.9	86.3	57.5	68.6	77.9
$CO_2$ @273 K	48.7(54.7)	38.7(33.5)	32.0	33.2	36.9	21.6	32.6	33.7
$CH_4$ @273 K	15.0(16.7)	12.1(9.8)	9.8	10.5	14.7	7.8	10.1	10.9

[a] data for materials prepared at room temperature are given in parentheses.

**BP1** is only slightly higher than for **BP2** (98.5 vs. 88.5 cm<sup>3</sup> g<sup>-1</sup> STP,  $P=850$  torr) which implies a much higher H<sub>2</sub> versus N<sub>2</sub> sorption selectivity in favor of the latter material (Table 2). In case of **BP1-Pd(PS)** and **BP2-Pd(PS)** the N<sub>2</sub> uptake was decreased. This effect was stronger for the latter material (485 cm<sup>3</sup> g<sup>-1</sup> STP for **BP1-Pd(PS)** vs. 71 cm<sup>3</sup> g<sup>-1</sup> STP for **BP2-Pd(PS)**). The sorption of H<sub>2</sub> was also lowered (86.3 and 57.5 cm<sup>3</sup> g<sup>-1</sup> STP for **BP1-Pd(PS)** and **BP2-Pd(PS)**, respectively,  $P=850$  torr) but to a lesser extent. This suggests the microporous structure was not strongly deteriorated by an introduction of Pd<sup>0</sup> centers on the surface of original materials **BP1-2**.

Nitrogen sorption of hybrid materials **BP1-Pd(BU)** and **BP2-Pd(BU)** was much lower (ca. two-fold) compared to their non-palladium counterparts **BP1-2** (Table 2). However, H<sub>2</sub> uptakes for **BP2** and **BP2-Pd(BU)** are in fact comparable (88.5 vs. 77.9 cm<sup>3</sup> g<sup>-1</sup> STP, respectively,  $P=850$  torr) which shows that introduction of Pd centers seems to be beneficial in terms of H<sub>2</sub>/N<sub>2</sub> sorption selectivity.

Investigation of the sorption properties of **BPO1-2** revealed that their N<sub>2</sub> uptake at 77 K amounts to ca. 100 cm<sup>3</sup> g<sup>-1</sup> STP at  $P/P_0=1$ , i.e., it was significantly lower compared to their analogues with P<sup>III</sup> centers. The sorption of H<sub>2</sub>@77 K was also lower relative to **BP1-2** but the difference was much smaller by the factors of ca. 1.5 and 1.1 for **BPO1-2**, respectively (Figure S51). This is consistent with an increased H<sub>2</sub>/N<sub>2</sub> uptake ratio for **BPO1-2** relative to **BP1-2**. This can be attributed to structural peculiarity due to the presence (and perhaps cooperation) of donor (P=O motif) and acceptor (B atom) sites.

The sorption of CO<sub>2</sub> and CH<sub>4</sub> was investigated at 273 and 293 K. For **BP1-2**, the sorption of CO<sub>2</sub> is at a moderate level (ca. 50 and 30 cm<sup>3</sup> g<sup>-1</sup> STP @273 K at  $P=P_0$ ) and is much higher than for CH<sub>4</sub> and N<sub>2</sub> (Figure 5 d). The isosteric heats of adsorption of CO<sub>2</sub> and CH<sub>4</sub> for higher degrees (>0.3) of surface coverage equal to ca. 27 and 20 kJ mol<sup>-1</sup>, respectively, and thus they are comparable to values found for most COFs. The sorption of CO<sub>2</sub> and CH<sub>4</sub> were also studied with Pd-functionalized COFs as well as **BPO1-2**. In all cases gas uptake was lower which can be ascribed to reduced porosity. Furthermore, coordination of Pd<sup>0</sup> centers or oxidation of phosphorus centers did not result in a significant change of CO<sub>2</sub>/CH<sub>4</sub> selectivity relative to **BP1-2**.

Laboratory PXRD analyses of all obtained materials indicate their crystallinity is rather low. Nevertheless, we succeeded in performing such analyses for **BP1** COF using the synchrotron radiation ( $\lambda=0.178$  Å). The PXRD pattern of **BP1** displays several broad peaks at lower  $2\theta$  angle (Figure 6). We proposed several structural models and compared the generated PXRD patterns to the experimental one. The best fit was obtained with a 3D structure resembling the topology of COF-105 and COF-108 obtained from condensation of tetrahedral precursors M(4-B(OH)<sub>2</sub>Ph)<sub>4</sub> (M=C, Si) and HHTP as a trigonal linker.<sup>[9]</sup> However, in **BP1** 1/4 of connections are replaced by the lone electron pair of the phosphorus atom. This partially resembles the situation observed in COF materials reported by Dichtel and Bunck by co-condensation of tetrahedral C(4-B(OH)<sub>2</sub>Ph)<sub>4</sub> and truncated CR(4-B(OH)<sub>2</sub>Ph)<sub>3</sub> (R=*n*-C<sub>12</sub>H<sub>26</sub>, allyl).<sup>[55]</sup> In our case, the structure is even more labile and supposedly vulnerable for catena-

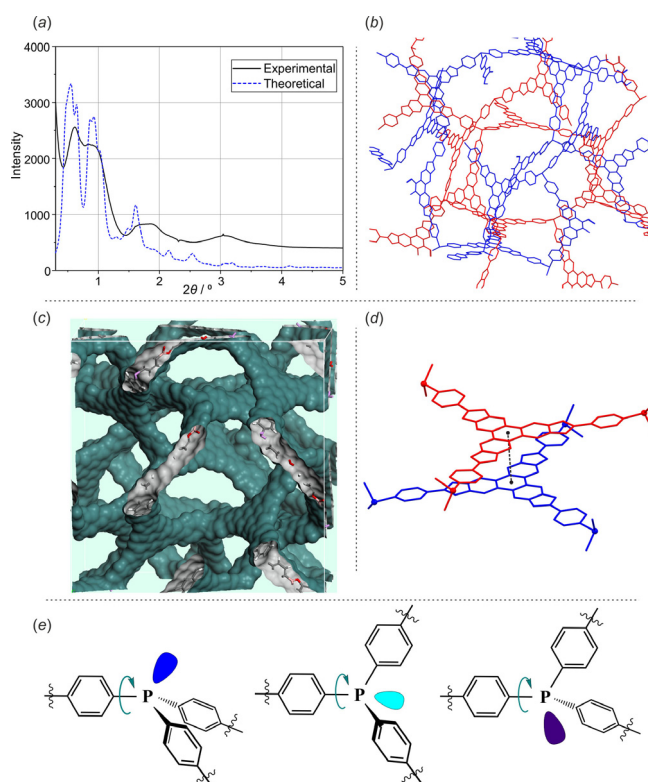


**Figure 6.** (a) Synchrotron-measured (black solid line) and simulated (blue dashed line) PXRD pattern of **BP1**. (b) Proposed structural model for the **BP1** material. (c) Connolly surface generated in the Mercury program; (d) two neighbored polymeric fragments are related by the symmetry center; (e) rotation around C–P bond as a source of structural disorder.

tion. In our model we proposed a two-fold interpenetration level, where two neighboring networks are related by the inversion center. However, a higher degree of catenation can also be considered. The PXRD pattern of **BP2** also shows some degree of structural ordering (Figure S37) which indicates that both materials can be categorized as COFs. We note, however, the proposed model should properly describe only the short-range order in this material. It seems the structures **BP1** and **BP2** are not strictly defined due to variable orientation of phosphorus centers leading to significant disorder and lack of well-defined long-range order.

In order to study the specificity of host-guest interactions in obtained materials, we have performed series of quantum chemical calculations at M062X/cc-pVTZ level of theory.<sup>[56,57]</sup> To simplify the calculations, the networks of **BP1** and **BPO1** were reduced to two closest fragments comprising organoboron and organophosphorus monomers with the initial distance between boron and P or P=O oxygen atoms set to 2.4 Å (**BP1'** and **BPO1'**). In the case of **BP1'** the geometry optimization led to the increase of the B...P distance to about 3.5 Å, meaning that moderate compatibility of phosphorus LP and boron free *p* orbital is insufficient to overcome the steric hindrance. In turn, in **BPO1'** the P=O...B distance was shortened to 2.11 Å resulting in appearance of dative P=O→B bond and slight pyramidalization of geometry around boron atom. The calculated interaction energy of 15.5 kJ mol<sup>-1</sup> suggests that BPOs would exhibit tendency for additional interconnections through the

ductive P=O→B interactions, but this effect seems to be too weak to organize the material into the well-defined crystal samples. Conversely, such a labile bond would rather decrease the ordering level.

Since polymer networks of **BP1** and **BPO1** are considered labile, it can be expected that Lewis base and acid centers would appear in the appropriate distance to invoke the local electric field effect, which could then enhance the interactions with guest molecules. The electrostatic potential maps plotted on electron density isosurfaces show strong electronegative regions around the phosphorus (**BP1'**) or P=O oxygen (**BPO1'**) atoms, while the slightly positive regions appear above the planes of boronate groups. (Figure S86). Due to rather low Lewis acidity of the boron atom, the expected binding effect would be rather weak and unsymmetrical with respect to classical frustrated Lewis pairs (FLPs).<sup>[58]</sup> It would be mostly dominated by the interaction with P<sup>III</sup>/P=O donor, and only supported by the interaction with boron atom. Indeed, the performed calculations on the host-guest systems confirms that the pres-

ence of boron and phosphorus centers supports binding of H<sub>2</sub>, CH<sub>4</sub> and CO<sub>2</sub> molecules by the framework, but this effect is insufficient to promote heterolytic bond splitting. The computed interaction energies clearly show that **BPO1'** displays higher affinity toward H<sub>2</sub> and CH<sub>4</sub> molecules, while **BP1'** strongly interacts ( $\Delta E = -33.4 \text{ kJ mol}^{-1}$ ) with CO<sub>2</sub> molecule. In line with these observations, the P/O...H (H<sub>2</sub>, CH<sub>4</sub>) distances are shorter in **BPO1'** and P=O...CO<sub>2</sub> distance is longer with respect to P...CO<sub>2</sub> in **BP1'** (Table 3). This can be simply understood by the higher basicity of oxygen atom, and stronger nucleophilic character of phosphorus atom.

The deeper insight into the host-guest binding mechanism is provided by the topological analysis of electron density in the framework of Bader's quantum theory of atoms in molecules (QTAIM).<sup>[59]</sup> Table 3 gathers the most important geometrical and electron density topological features of host-guest interactions. Molecular graphs showing the formation of bond paths and bond critical points (BCP) in the binding pocket are presented on Figure 7, full molecular graphs are given in SI

**Table 3.** Characterization of host-guest interaction energies.  $\Delta E$  denotes the interaction energy between host and guest molecule,  $d$  is interatomic distance between P/O, B and guest molecule XY (X,Y=H for H<sub>2</sub>, CH<sub>4</sub>; X=C and Y=O for CO<sub>2</sub>),  $\rho$  and  $\nabla^2\rho$  are electron density and its Laplacian at P/O...X (BPC1) and Y...B (BPC2) bond critical points.

Host	Guest	$\Delta E$ [kJ mol <sup>-1</sup> ]	$d_{\text{P/O-X}}$ [Å]	$d_{\text{B-Y}}$ [Å]	$d_{\text{P/O-B}}$ [Å]	$\rho(\text{BPC1})$ [eÅ <sup>-3</sup> ]	$\nabla^2\rho(\text{BPC1})$ [eÅ <sup>-5</sup> ]	$\rho(\text{BPC2})$ [eÅ <sup>-3</sup> ]	$\nabla^2\rho(\text{BPC2})$ [eÅ <sup>-5</sup> ]
<b>BP1</b>	H <sub>2</sub>	-1.1	2.503	2.273	4.850	0.12	1.02	0.09	0.94
	CO <sub>2</sub>	-33.4	2.393	3.155	6.014	0.41	0.80	0.03	0.46
	CH <sub>4</sub>	-0.8	2.835	2.426	6.483	0.07	0.57	0.07	0.69
<b>BPO1</b>	H <sub>2</sub>	-5.7	1.963	2.101	4.458	0.16	2.34	0.11	1.09
	CO <sub>2</sub>	-6.3	2.437	2.526	5.186	0.14	2.23	0.11	1.19
	CH <sub>4</sub>	-4.2	2.556	2.933	6.306	0.05	0.56	0.03 <sup>[a]</sup>	0.33 <sup>[a]</sup>

[a] BCP2 was found between C–H hydrogen and boronate ester oxygen atom.

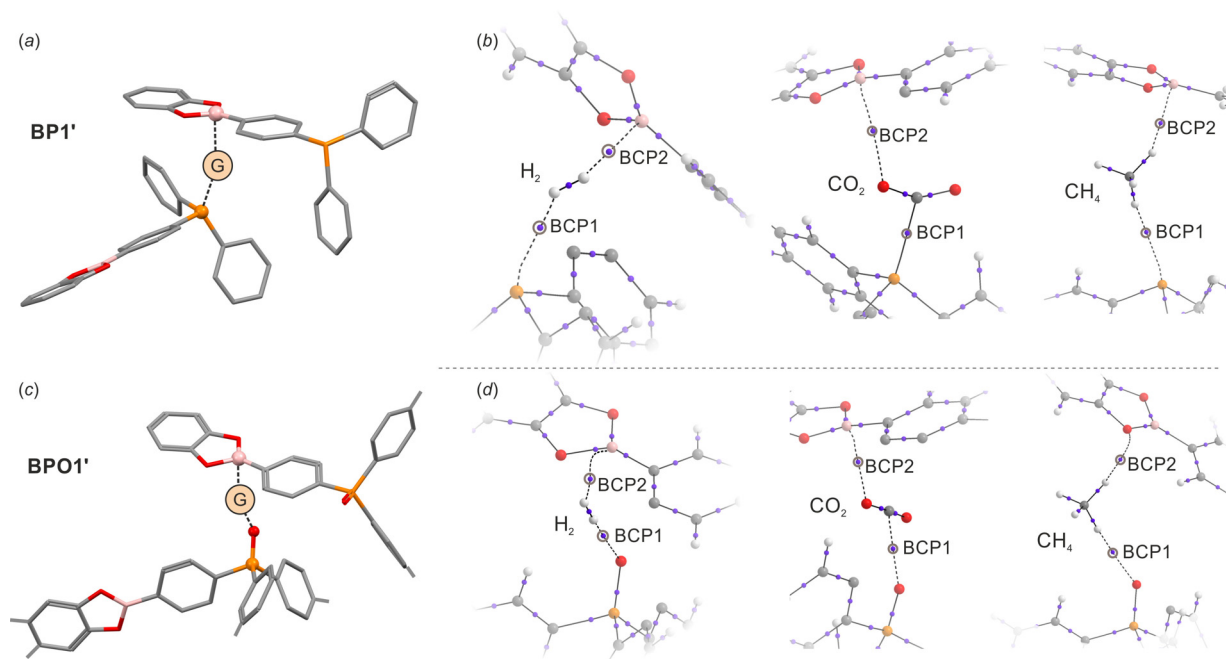


**Figure 7.** (a,c) Modelling of host-guest interactions in **BP1** and **BPO1** materials. (b,d) Fragment of molecular graphs showing bond paths (black dashed lines) and bond critical points (small blue spheres) in host-guest interaction region.



(Figures S87–S92). The topological analyses of electron density recognized bond paths and bond critical points (BCPs) between all donor centers and H ( $H_2$ ,  $CH_4$ ) or C ( $CO_2$ ) atoms from guest molecules. The electron density values follows the general trend observed for interatomic distances. Specifically, for **BPO1'**- $H_2$  adduct, where donor...H distance is the shortest from studied series ( $d_{O...H}=1.963$  Å), the electron density at P...H bond critical point reaches the value of  $0.16$  eÅ<sup>-3</sup> with negative Laplacian of  $2.34$  eÅ<sup>-5</sup> and host-guest interaction energy equals to  $-5.7$  kJ mol<sup>-1</sup> indicating that this interaction can be classified as weak hydrogen bond. As indicated by longer P...H distance (2.503 Å) and lower  $\rho(\text{BCP1})$  value of  $0.12$  eÅ<sup>-3</sup>, the binding of dihydrogen by **BP1'** is weaker ( $\Delta E = -1.1$  kJ mol<sup>-1</sup>), but still satisfies the criteria of very weak intermolecular hydrogen bond. In both cases, the donation from donor to  $H_2$  molecule results in elongation of H–H bond from  $0.744$  Å (equilibrium distance in free  $H_2$  calculated at the same level of theory) to  $0.761$  Å in **BP1'** and  $0.780$  Å in **BPO1'**, which is accompanied by the reduction of electron density at H–H BCP from  $1.84$  eÅ<sup>-3</sup> to  $1.81$  eÅ<sup>-3</sup> (**BP1'**) and  $1.68$  eÅ<sup>-3</sup> (**BPO1'**). Our observations are somewhat consistent with theoretical studies conducted by Pinter et al.<sup>[60]</sup> on FLPs featuring low-energy dihydrogen activation transition states termed “early” (such as  $tBu_3P\cdot B(C_6F_5)_3$ ). In contrast to so-called “late” FLPs, such “early” complexes are characterized by relatively short H–H distances ( $0.79$ – $0.80$  Å), slightly decreased electron density at  $H_2$  BCP ( $1.6$  eÅ<sup>-3</sup>), long P...H distances and electron density values at BCPs of P...H bond in the range of  $0.2$ – $0.3$  eÅ<sup>-3</sup>. Nonetheless, “early” FLPs systems are active hydrogenation catalysts. The comparison between FLPs and our systems leads to the conclusion that in the latter the donor binding effect is weaker presumably due to the lack of strong support from acceptor side. Although, topological analysis of electron density revealed the formation of H...B bond path in both models **BP1'** and **BPO1'**, the value of electron density at BCP2 oscillates near  $0.1$  eÅ<sup>-3</sup> and it is more than two times smaller with respect to “early”  $tBu_3P\cdot H_2\cdot B(C_6F_5)_3$  complex. On the other hand, the lower activity of **BP1'** and **BPO1'** is compensated by the higher stability of formed host-guest adducts.

An interesting observation can be made by the comparison of interatomic distances and electron density features of B...H versus donor  $P^{III}/P=O\cdots H$  interactions with dihydrogen and methane. Despite the C–H bond polarization, the donor...H interactions are weaker with methane than dihydrogen. It should be also noted that in case of the **BPO1'**- $CH_4$  bond path was recognized between C–H hydrogen atom and oxygen atom from boronate ester group with electron density of only  $0.03$  eÅ<sup>-3</sup> at BCP2. Thus the contribution from boron atom is questionable. Regardless of binding mechanism, the C–H bonds from donor and acceptor sites are elongated and electron density depleted at BCP with respect to free  $CH_4$  molecule. Furthermore, the calculations show that both  $H_2$  and  $CH_4$  adducts are unstable in the absence of boron counterparts.

The **BP1'**- $CO_2$  is the most distinct adduct from the studied series. The exceptionally high value of electron density at P... $CO_2$  BCP of  $0.46$  eÅ<sup>-3</sup> confirms the strong character of this interaction and points to the chemical nature of  $CO_2$  adsorp-

tion. This also leads to the significant bending of  $CO_2$  molecule ( $\alpha_{O-C-O}=153^\circ$ ), elongation of C–O bond (from  $1.155$  Å to  $1.178$  Å), and reduction of electron density at corresponding BCP (from  $3.158$  eÅ<sup>-3</sup> to  $3.038$  eÅ<sup>-3</sup>) with respect to free  $CO_2$  molecule. On the other hand, the boron atom is barely involved. Turning to less nucleophilic phosphine oxide, the interaction energy with  $CO_2$  ( $\Delta E = -6.3$  kJ mol<sup>-1</sup>) and the amount of electron density localized at BCP1 ( $0.14$  eÅ<sup>-3</sup>) are comparable to **BPO1'**- $H_2$  adduct. Accordingly, the geometry of  $CO_2$  molecule approach to linear with the O–C–O angle of  $171^\circ$ . Interestingly, the formation of moderate  $P=O\cdots CO_2$  interaction is accompanied by the increased contribution from boron atom reflected by relatively short B...O contact ( $2.526$  Å) and electron density value of  $0.11$  eÅ<sup>-3</sup> at BCP2.

The analysis of Hirshfeld<sup>[61]</sup> and Bader<sup>[59]</sup> atomic charges revealed that the charge is transferred from donor to guest molecule, however, it is only partially transferred further to acceptor unit (Tables S2 and S3). For most systems, the population at the donor atom ( $P^{III}/P=O$ ) drops by  $0.02$ – $0.04$  e (Hirshfeld charges), while the magnitude of charge donation from the guest molecule to the boron atom is of about  $0.005$ – $0.025$  e. In line with previous findings, the magnitude of charge transfer from **BP1'** donor to  $CO_2$  molecule is larger. The charge at P atom is depleted by ca.  $0.1$  e, while guest molecule and boron atom increase electron population by  $0.162$  e and  $0.025$  e, respectively. It is also noticeable that charge is distributed unsymmetrically within the guest molecule, wherein it is mostly shifted toward the acceptor hydrogen ( $H_2$ ,  $CH_4$ ) or carbon ( $CO_2$ ) atoms. This again emphasizes the dominant character of  $P^{III}/P=O$  donor site in the binding processes.

## Conclusions

We have demonstrated that the general approach to phosphine coordination materials mostly developed for MOF family can be successfully extended to covalent organic frameworks. The transesterification of triboronated triphenylphosphine **2** and its oxide **4** esters with polyhydroxy HHTP and THDMA linkers is a facile route toward the formation of boron-phosphine COFs that are characterized by higher selectivity toward  $H_2$ ,  $CH_4$  and  $CO_2$ . The tripodal topology of the employed boronic linkers stems from the presence of the phosphorus(III) center. Obtained materials display lower crystallinity with respect to related boron COF materials resulting from fast transesterification rates and statistically random orientation of phosphorus center with respect to three aryl substituents and lone electron pair. However, synchrotron radiation experiments revealed some short-range structure ordering. The proposed **BP1** structural model assumes two-fold interpenetration level and general topology preserved from COF-105, but it is characterized by higher flexibility and ordering discontinuity.

The BET surfaces derived from nitrogen sorption isotherm are moderate. However, obtained materials exhibit uptakes of hydrogen,  $CO_2$  and methane at a level similar to those found for boron COFs featuring higher  $N_2$ -based  $S_{BET}$  values. In other words, the obtained porous materials have much higher relative affinity with respect to  $H_2$ ,  $CO_2$  and  $CH_4$  than standard

boron COFs. We suppose that this effect can be ascribed to the presence of boron Lewis acidic and phosphorus Lewis basic centers which is beneficial for binding of more polarizable molecules due to generation of local electric field gradients. These suppositions has been confirmed by theoretical calculations. The interaction with gaseous molecules has some common features with “early” FLP systems reflected by slightly decreased distance and electron density at BCP of H–H bond, elongated donor–guest distances with electron density localized at corresponding BPC ranging from 0.2–0.3 eÅ<sup>-3</sup> and 0.02–0.04 e charge transferred from basic center to guest molecule. On the other hand the contribution of Lewis acidic boron atom is less pronounced. Thus, an overall effect is beneficial for sorption effectiveness but it is insufficient to promote stronger host-guest interactions or bond splitting. In contrast, theoretical calculations suggest that CO<sub>2</sub> is bound by **BP1** more effectively due to stronger nucleophilic character of P<sup>III</sup> atom and intrinsic polarity of C=O bonds.

Post-synthetic modification of the materials was performed by impregnation with Pd<sub>2</sub>(dba)<sub>3</sub> in DCM. XPS analyses demonstrated that the presence of phosphorus donor centers results in a strong affinity to Pd<sup>0</sup> leading to the high Pd/P ratio of ca. 0.9. Incorporation of the metal resulted in significant decrease of the BET surface. However, there is still space left available for uptake of guest molecules. In a different bottom-up approach, the precursor **1** was first reacted with Pd<sub>2</sub>(dba)<sub>3</sub> followed by polycondensation with HHTP or THDMA. Thus the resulting materials possess the hybrid character due to presence of Pd–P dative bonds as well as boronate ester moieties typical of boron COFs. The sorption properties of these amorphous networks are slightly worse than those found for **BP1–2**. According to XPS analyses, the obtained materials exhibit much lower surface Pd/P ratio of 0.26–0.31 consistent with the assumed stoichiometry of the Pd complex used as a precursor. All obtained Pd-containing porous materials could potentially serve as heterogeneous catalysts, e.g., for hydrogenation and cross-coupling reactions. We will test such applications in our future approaches.

## Acknowledgements

This work was supported by National Science Centre in Poland (grant No. 2016/21/B/ST5/00118). Authors thank J. Lewiński (WUT, Warsaw, Poland) for providing access to the physisorption analyzer, K. Woźniak (UW, Warsaw, Poland) for providing access to the single-crystal X-ray diffraction facility, A. Ostrowski (WUT, Warsaw, Poland) for providing access to the PXRD machine, P. Wicziński and T. Płociński (WUT, Warsaw, Poland) for providing access to the SEM setup. PXRD synchrotron X-ray diffraction experiments were performed at the ID11 beamline of the European Synchrotron Radiation Facility (ESRF), Grenoble, France. K. N. Jarzemska (UW, Warsaw, Poland) is thanked with preparing beamline proposal, and A. Poulain and C. Giacobbe (ESRF, Grenoble, France) for support on the experiments. The access to ESRF was financed by the Polish Ministry of Science and High Education (decision No. DIR/WK/2016/19).

Computational facilities were provided by the Wrocław Centre for Networking and Supercomputing (grant No. 285) and the work has been performed under the Project HPC-EUROPA3 (INFRAIA-2016-1-730897), with the support of the EC Research Innovation Action under the H2020 program; in particular, K.D. gratefully acknowledges the support of T. Düren and G. Donval from the Department of Chemical Engineering, University of Bath, UK, the computer resources and technical support provided by EPCC (University of Edinburgh, UK) and M. Antonietti for his support during this project.

## Conflict of interest

The authors declare no conflict of interest.

**Keywords:** coordination polymers · covalent organic frameworks · frustrated Lewis pairs · quantum nature of host-guest interactions · structural modeling

- [1] X. Feng, X. Ding, D. Jiang, *Chem. Soc. Rev.* **2012**, *41*, 6010–6022.
- [2] S.-Y. Ding, W. Wang, *Chem. Soc. Rev.* **2013**, *42*, 548–568.
- [3] P. J. Waller, F. Gándara, O. M. Yaghi, *Acc. Chem. Res.* **2015**, *48*, 3053–3063.
- [4] Z. Xiang, D. Cao, L. Dai, *Polym. Chem.* **2015**, *6*, 1896–1911.
- [5] N. Huang, P. Wang, D. Jiang, *Nat. Rev. Mater.* **2016**, *1*, 16068.
- [6] H. Furukawa, O. M. Yaghi, *J. Am. Chem. Soc.* **2009**, *131*, 8875–8883.
- [7] A. P. Côté, A. I. Benin, N. W. Ockwig, M. O’Keeffe, A. J. Matzger, O. M. Yaghi, *Science* **2005**, *310*, 1166–1170.
- [8] A. P. Côté, H. M. El-Kaderi, H. Furukawa, J. R. Hunt, O. M. Yaghi, *J. Am. Chem. Soc.* **2007**, *129*, 12914–12915.
- [9] H. M. El-Kaderi, J. R. Hunt, J. L. Mendoza-Cortés, A. P. Côté, R. E. Taylor, M. O’Keeffe, O. M. Yaghi, *Science* **2007**, *316*, 268–272.
- [10] S. M. Humphrey, P. K. Allan, S. E. Oungoulian, M. S. Ironside, E. R. Wise, *Dalton Trans.* **2009**, 2298–2305.
- [11] S. M. Humphrey, S. E. Oungoulian, J. W. Yoon, Y. K. Hwang, E. R. Wise, J.-S. Chang, *Chem. Commun.* **2008**, 2891–2893.
- [12] A. J. Nuñez, L. N. Shear, N. Dahal, I. A. Ibarra, J. Yoon, Y. K. Hwang, J.-S. Chang, S. M. Humphrey, *Chem. Commun.* **2011**, *47*, 11855–11857.
- [13] A. J. Nuñez, M. S. Chang, I. A. Ibarra, S. M. Humphrey, *Inorg. Chem.* **2014**, *53*, 282–288.
- [14] A. M. Bohnsack, I. A. Ibarra, P. W. Hatfield, J. W. Yoon, Y. K. Hwang, J.-S. Chang, S. M. Humphrey, *Chem. Commun.* **2011**, *47*, 4899–4901.
- [15] A. M. Bohnsack, I. A. Ibarra, V. I. Bakhmutov, V. M. Lynch, S. M. Humphrey, *J. Am. Chem. Soc.* **2013**, *135*, 16038–16041.
- [16] I. A. Ibarra, K. E. Tan, V. M. Lynch, S. M. Humphrey, *Dalton Trans.* **2012**, *41*, 3920–3923.
- [17] I. A. Ibarra, T. W. Hesterberg, B. J. Holliday, V. M. Lynch, S. M. Humphrey, *Dalton Trans.* **2012**, *41*, 8003–8009.
- [18] I. A. Ibarra, T. W. Hesterberg, J.-S. Chang, J. W. Yoon, B. J. Holliday, S. M. Humphrey, *Chem. Commun.* **2013**, *49*, 7156–7158.
- [19] I. A. Ibarra, J. W. Yoon, J.-S. Chang, S. K. Lee, V. M. Lynch, S. M. Humphrey, *Inorg. Chem.* **2012**, *51*, 12242–12247.
- [20] N. W. Waggoner, B. Saccoccia, I. A. Ibarra, V. M. Lynch, P. T. Wood, S. M. Humphrey, *Inorg. Chem.* **2014**, *53*, 12674–12676.
- [21] A. A. Bezrukov, P. D. C. Dietzel, *Inorg. Chem.* **2017**, *56*, 12830–12838.
- [22] A. A. Bezrukov, K. W. Törnroos, P. D. C. Dietzel, *Cryst. Growth Des.* **2017**, *17*, 3257–3266.
- [23] A. A. Bezrukov, K. W. Törnroos, E. L. Roux, P. D. C. Dietzel, *Chem. Commun.* **2018**, *54*, 2735–2738.
- [24] J. E. Reynolds, A. M. Bohnsack, D. J. Kristek, A. Gutiérrez-Alejandre, S. G. Dunning, N. W. Waggoner, R. E. Sikma, I. A. Ibarra, S. M. Humphrey, *J. Mater. Chem. A* **2019**, *7*, 16842–16849.
- [25] J. E. Reynolds, K. M. Walsh, B. Li, P. Kunal, B. Chen, S. M. Humphrey, *Chem. Commun.* **2018**, *54*, 9937–9940.

- [26] S. Wu, C. Teng, S. Cai, B. Jiang, Y. Wang, H. Meng, H. Tao, *Nanoscale Res. Lett.* **2017**, *12*, 609.
- [27] D. Marcoux, A. B. Charette, *J. Org. Chem.* **2008**, *73*, 590–593.
- [28] R. Davies, *Handb. Chalcogen Chem.* **2006**, pp. 286–343.
- [29] T. Bartik, B. Bartik, B. E. Hanson, K. H. Whitmire, I. Guo, *Inorg. Chem.* **1993**, *32*, 5833–5837.
- [30] T. Drake, P. Ji, W. Lin, *Acc. Chem. Res.* **2018**, *51*, 2129–2138.
- [31] J. Václavík, M. Servalli, C. Lothschütz, J. Szlachetko, M. Ranocchiaro, J. A. van Bokhoven, *ChemCatChem* **2013**, *5*, 692–696.
- [32] S. G. Dunning, J. E. Reynolds, K. M. Walsh, D. J. Kristek, V. M. Lynch, P. Kunal, S. M. Humphrey, *Organometallics* **2019**, *38*, 3406–3411.
- [33] R. J. Young, M. T. Huxley, E. Pardo, N. R. Champness, C. J. Sumbly, C. J. Doonan, *Chem. Sci.*, **2020**, *11*, 4031–4050.
- [34] S. G. Dunning, G. Nandra, A. D. Conn, W. Chai, R. E. Sikma, J. S. Lee, P. Kunal, J. E. Reynolds, J.-S. Chang, A. Steiner, G. Henkelman, S. M. Humphrey, *Angew. Chem. Int. Ed.* **2018**, *57*, 9295–9299; *Angew. Chem.* **2018**, *130*, 9439–9443.
- [35] O. Mabayoje, S. G. Dunning, K. Kawashima, B. R. Wygant, R. A. Ciufu, S. M. Humphrey, C. B. Mullins, *ACS Appl. Energy Mater.* **2020**, *3*, 176–183.
- [36] K. Gontarczyk, W. Bury, J. Serwatowski, P. Wieciński, K. Woźniak, K. Durka, S. Luliński, *ACS Appl. Mater. Interfaces* **2017**, *9*, 31129–31141.
- [37] P. Tomaszewski, M. Wiszniewski, K. Gontarczyk, P. Wieciński, K. Durka, S. Luliński, *Polymers* **2019**, *11*, 1070.
- [38] R. Amengual, E. Genin, V. Michelet, M. Savignac, J.-P. Genêt, *Adv. Synth. Catal.* **2002**, *344*, 393–398.
- [39] J. N. Smith, J. M. Hook, N. T. Lucas, *J. Am. Chem. Soc.* **2018**, *140*, 1131–1141.
- [40] S. Klotzbach, F. Beuerle, *Angew. Chem. Int. Ed.* **2015**, *54*, 10356–10360; *Angew. Chem.* **2015**, *127*, 10497–10502.
- [41] T. Lorenz, A. Lik, F. A. Plamper, H. Helten, *Angew. Chem. Int. Ed.* **2016**, *55*, 7236–7241; *Angew. Chem.* **2016**, *128*, 7352–7357.
- [42] B. E. Mann, A. Musco, *J. Chem. Soc. Dalton Trans.* **1975**, 1673–1677.
- [43] S. Zhang, Q. Liu, M. Shen, B. Hu, Q. Chen, H. Li, J.-P. Amoureux, *Dalton Trans.* **2012**, *41*, 4692–4698.
- [44] S. A. Burgess, A. Kassie, S. A. Baranowski, K. J. Fritzsching, K. Schmidt-Rohr, C. M. Brown, C. R. Wade, *J. Am. Chem. Soc.* **2016**, *138*, 1780–1783.
- [45] J. W. E. Weiss, D. L. Bryce, *J. Phys. Chem. A* **2010**, *114*, 5119–5131.
- [46] W. P. Power, *J. Am. Chem. Soc.* **1995**, *117*, 1800–1806.
- [47] T. Wiegand, H. Eckert, O. Ekkert, R. Fröhlich, G. Kehr, G. Erker, S. Grimme, *J. Am. Chem. Soc.* **2012**, *134*, 4236–4249.
- [48] G. Maheut, M. Hervieu, C. Fernandez, V. Montouillout, D. Villemin, P.-A. Jaffrès, *J. Mol. Struct.* **2003**, *659*, 135–142.
- [49] C. Andersson, R. Larsson, *J. Catal.* **1983**, *81*, 194–203.
- [50] M. C. Militello, S. J. Simko, *Surf. Sci. Spectra* **1994**, *3*, 387–394.
- [51] M. Vanni, M. Serrano-Ruiz, F. Telesio, S. Heun, M. Banchelli, P. Matteini, A. M. Mio, G. Nicotra, C. Spinella, S. Caporali, M. Peruzzini, *Chem. Mater.* **2019**, *31*, 5075–5080.
- [52] T. Horikawa, D. D. Do, D. Nicholson, *Adv. Colloid Interface Sci.* **2011**, *169*, 40–58.
- [53] J. Rouquerol, P. Llewellyn, F. Rouquerol, in *Stud. Surf. Sci. Catal.*, Elsevier, **2007**, pp. 49–56.
- [54] M. Dogru, A. Sonnauer, A. Gavryushin, P. Knochel, T. Bein, *Chem. Commun.* **2011**, *47*, 1707.
- [55] D. N. Bunck, W. R. Dichtel, *Angew. Chem. Int. Ed.* **2012**, *51*, 1885–1889; *Angew. Chem.* **2012**, *124*, 1921–1925.
- [56] Y. Zhao, D. G. Truhlar, *Theor. Chem. Acc.* **2008**, *120*, 215–241.
- [57] T. H. Dunning, *J. Chem. Phys.* **1989**, *90*, 1007–1023.
- [58] D. W. Stephan, *Acc. Chem. Res.* **2015**, *48*, 306–316.
- [59] R. F. W. Bader, *Atoms in Molecules: A Quantum Theory*, Oxford University Press, Oxford, New York, **1994**.
- [60] G. Skara, F. De Vleeschouwer, P. Geerlings, F. De Proft, B. Pinter, *Sci. Rep.* **2017**, *7*, 16024.
- [61] F. L. Hirshfeld, *Theor. Chim. Acta* **1977**, *44*, 129–138.

Manuscript received: April 22, 2020

Revised manuscript received: May 25, 2020

Accepted manuscript online: May 28, 2020

Version of record online: September 1, 2020